Inorganic Chemistry

Article

pubs.acs.org/IC

Synthesis, Structure, and Properties of the Electron-Poor II–V Semiconductor ZnAs

Andreas Fischer,[†] Daniel Eklöf,[‡] Daryn E. Benson,[§] Yang Wu,[∥,⊥] Ernst-Wilhelm Scheidt,[†] Wolfgang Scherer,[†] and Ulrich Häussermann*[,‡]

[†]Department of Physics, Augsburg University, D-86135 Augsburg, Germany

[‡]Department of Materials and Environmental Chemistry, Stockholm University, S-10691 Stockholm, Sweden

[§]Department of Physics and [∥]Department of Chemistry & Biochemistry, Arizona State University, Tempe, Arizona 85287, United States

Supporting Information

ABSTRACT: ZnAs was synthesized at 6 GPa and 1273 K utilizing multianvil high-pressure techniques and structurally characterized by single-crystal and powder X-ray diffraction (space group *Pbca* (No. 61), a = 5.6768(2) Å, b = 7.2796(2) Å, c = 7.5593(2) Å, Z = 8). The compound is isostructural to ZnSb (CdSb type) and displays multicenter bonded rhomboid rings Zn_2As_2, which are connected to each other by classical two-center, two-electron bonds. At ambient pressure ZnAs is metastable with respect to Zn_3As_2 and $ZnAs_2$. When heating at a rate of 10 K/min decomposition takes place at ∼700 K. Diffuse reflectance measurements reveal a band gap of 0.9 eV. Electrical resistivity, thermopower, and thermal conductivity were measured in the temperature range of 2–400 K and compared to thermoelectric ZnSb. The room temperature values of the resistivity and thermopower are ∼1 Ω cm and +27 μV/K, respectively. These values are considerably higher and lower, respectively, compared to ZnSb. Above 150 K the thermal conductivity attains low values, around 2 W/m·K, which is similar to that of ZnSb. The heat capacity of ZnAs was measured between 2 and 300 K and partitioned into a Debye and two Einstein contributions with temperatures of θ_D = 234 K, θ_{E1} = 95 K, and θ_{E2} = 353 K. Heat capacity and thermal conductivity of ZnSb and ZnAs show very similar features, which possibly relates to their common electron-poor bonding properties.

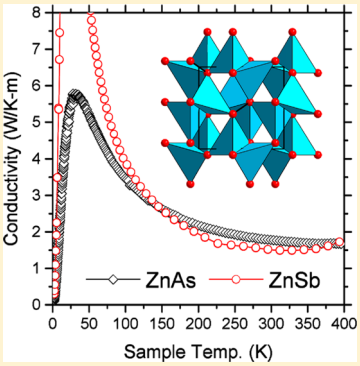

1. INTRODUCTION

The binary Zn–Sb system has a peculiar phase diagram where three fields of phases are located in the narrow range between 50 and 60 atom % Zn (ZnSb, Zn_4Sb_3, and Zn_3Sb_2).[1,2] Zn_4Sb_3 exhibits one of the highest thermoelectric figures of merit known for a binary compound and has been intensely investigated.[3−5] Lately also ZnSb has been recognized as a high-performance thermoelectric material.[6−8] Zn_3Sb_2 is metastable at room temperature, and its properties are not well-characterized. Moving from the Zn–Sb to the Zn–As system there are remarkable changes: in the ambient-pressure Zn–As phase diagram ZnAs and Zn_4As_3 are absent, and congruently melting $ZnAs_2$ and Zn_3As_2 represent the only phases.[2]

According to earlier reports equiatomic ZnAs is accessible either from the pressure-induced decomposition of $ZnAs_2$ or Zn_3As_2 or from the direct reaction of the elements at high-pressure, high-temperature conditions.[9,10] Earlier work did not address the physical properties of ZnAs. Recently we investigated the bonding properties and electronic structure of ZnAs in a computational study.[11] Similar to ZnSb, ZnAs possesses an indirect band gap, but its size remains uncertain. Because of the increasing interest in ZnSb as a thermoelectric material we deemed it important to obtain more information on synthesis, structure, and physical properties of isostructural ZnAs.

Generally II–V semiconductors (II = Zn, Cd; V = P, As, Sb) display interesting, often anisotropic transport properties.[12−15] Compared to the well-investigated tetrahedrally bonded II–VI and III–V compound semiconductors, crystal structures and bonding properties are far more complex and less understood. It is not immediately apparent why band gaps should actually should occur given the fact that the average electron concentration of many II–V systems is lower than four.[16] Other peculiarities include a very low lattice thermal conductivity, which is especially observed for Zn_4Sb_3 and ZnSb and is a major reason for the favorable thermoelectric performance of these materials. The origin of the low lattice thermal conductivity of Zn_4Sb_3 and ZnSb is still debated,[4−6] and the study of ZnAs may provide new insight.

2. EXPERIMENTAL METHODS

Synthesis. Zn (shot, 99.99%) and As (pieces, 99.999%) from Sigma-Aldrich were weighed in atomic ratios between 0.45:0.55 and 0.55:0.45 and pressed into pellets in an argon-filled glovebox. Pellets were then placed in a threaded BN capsule (0.8 mm wall thickness, 4.5

Received: June 5, 2014
Published: July 28, 2014

   dx.doi.org/10.1021/ic501308q | *Inorg. Chem.* 2014, 53, 8691−8699

Table 1. Summary of Crystallographic Data and Structural Analysis for ZnAs

	ZnAs 100 K		ZnAs 300 K
formula		ZnAs	
crystal system		orthorhombic	
space group		*Pbca*, No. 61 ITC	
a, Å	5.6607(3)		5.6730(1)
b, Å	7.2774(4)		7.2754(2)
c, Å	7.5605(5)		7.5572(2)
V, Å^3	311.43(3)		311.916(13)
ρ (g/cm^3)	5.9827		5.9735
Z		8	
*F*000		504	
crystal size		0.041 × 0.072 × 0.074	
μ(Ag Kα), mm^{-1}	19.009		18.979
T, K	100(2)		300(2)
radiation		Ag Kα	
θ range (deg)	$4.18 < \theta < 30.54$		$4.18 < \theta < 30.60$
sin θ/λ_{max}	0.906		0.908
data collected (*h*, *k*, *l*)	$-9 < h < 10$, $-12 < k < 12$, $-13 < l < 13$		$-10 < h < 10$, $-12 < k < 13$, $-13 < l < 13$
no. of reflns measured	13 833		15 257
no. of unique reflns	928		930
no. of observed reflns, $I > 3\sigma(I)$	874		843
no. of refined parameters		20	
extinction		type 2 isotropic	
ρ_{iso}	0.08(2)		0.06(2)
R_{int}	4.24		4.17
R_1 $I > 3\sigma(I)$	1.52		1.58
wR_1 $I > 3\sigma(I)$	2.25		2.18
GOF on *F*	1.43		1.36
largest peak/hole e/Å^3	+1.08/−0.76		+0.75/−0.69
absorption correction		numerical, face-indexed	
transmission min, max	0.3649, 0.6278		0.3671, 0.6212

mm inner diameter), which was closed by screwing on a BN lid. The threading provided a reasonable airtight seal for the reaction mixture. Subsequently capsules were transferred outside the glovebox. High-pressure syntheses were performed in a 6−8 multianvil high-pressure device using an 18/12 assembly developed by Stoyanov et al.[17] BN sample capsules were positioned in a graphite furnace that, in turn, was placed together with a zirconia thermal insulating sleeve (0.57 mm wall thickness, 7.77 mm OD, 10.80 mm length) in a magnesia octahedron with 18 mm edge length. Samples were pressurized at a rate of about 0.5 GPa/h with 25 mm tungsten carbide cubes truncated to 12 mm edge length. After reaching the target pressure (between 4 and 6 GPa) the samples were heated. Deviations from the target pressure are estimated as ±0.3 GPa. The temperature was measured close to the sample using a thermocouple type C (W5%Re − W26%Re wire) in an Al_2O_3 sleeve.

To prevent blowouts, heating was done very carefully. The following protocol was established: (i) temperature was raised to 673 K at a rate of 10 K/min and kept there for 15 min, (ii) temperature was raised to 873 K at a rate of 5 K/min and kept there for 30 min, (iii) temperature was raised to 1073 K at a rate of 5 K/min and kept there for 15 min, (iv) temperature was raised to 1273 K at a rate of 5 K/min. After a dwell time of 15 min, the samples were quenched at approximately constant pressure by turning off the power to the furnace (initial quench rate ≈ 50 °C/s). Afterward, the pressure was released at a rate of approximately 0.5 GPa/h, and samples were recovered. A variety of reaction parameters (temperature, pressure, dwell time, Zn/As ratio) were explored. Phase-pure samples of ZnAs resulted from a starting mixture of 51.5 atom % As and 48.5 atom % Zn being reacted at 6 GPa and 1273 K. Products were obtained as dense cylinders with approximate dimensions of 4.5 mm o.d. and 4.2 mm height. Cylinders were partially crushed and ground for subsequent sample analysis.

Sample Analysis. Powder X-ray diffraction (PXRD) patterns were collected on a Panalytical X'Pert PRO diffractometer operated with Cu Kα_1 radiation and in $\theta-2\theta$ diffraction geometry. Powdered samples were applied to a zero diffraction plate and diffraction patterns measured in a 2θ range of 20−80°.

Rietveld refinement using the Jana2006 package[18] was performed to determine the phase fraction of impurities. A summary of the refinement results is given as Supporting Information (Table S1). Scanning electron microscopy (SEM) investigations were performed on a JEOL JSM-7000F instrument to examine the microstructure and compositional homogeneity of ZnAs specimens. Samples were first polished mechanically and then with an Ar$^+$-ion beam in a Cross Section Polisher SM-09011 instrument from JEOL. Backscattered electron images were recorded with an acceleration voltage of 8 kV. According to a simulation of electron trajectory (program CASINO)[19] this voltage yields an information depth of 75−100 nm. For energy-disperse X-ray spectrometry (EDX) an X-ray detector from Oxford instruments, INCA X-sight, was used. The density of samples was determined by measuring their volume with a gas (He) expansion pycnometer (AccuPyc 1330 from Micromeretics). The instrument was calibrated, and its accuracy was confirmed with pieces of crystalline Si of similar volume as the ZnAs samples. Errors in determined densities are estimated to be less than 0.2%.

Thermal Analysis. 10.03 mg of ZnAs was sealed in an aluminum pan. Differential scanning calorimetry (DSC) was performed using a PerkinElmer Pyris 1 "heat flux" calorimeter under a nitrogen gas flow of ∼20 mL/min. The scanning range was from 473 to 773 K with a heating/cooling rate of 10 K/min. A baseline calibration was performed to compensate for the cell heat flow imbalance between reference and sample positions. Temperature and heat flow were calibrated using indium (T_m = 429.8 K, ΔH_{fus} = 28.4 J/g) and tin (T_m = 505.1 K). DSC curves and enthalpy of transitions were accessed with

dx.doi.org/10.1021/ic501308q | Inorg. Chem. 2014, 53, 8691−8699

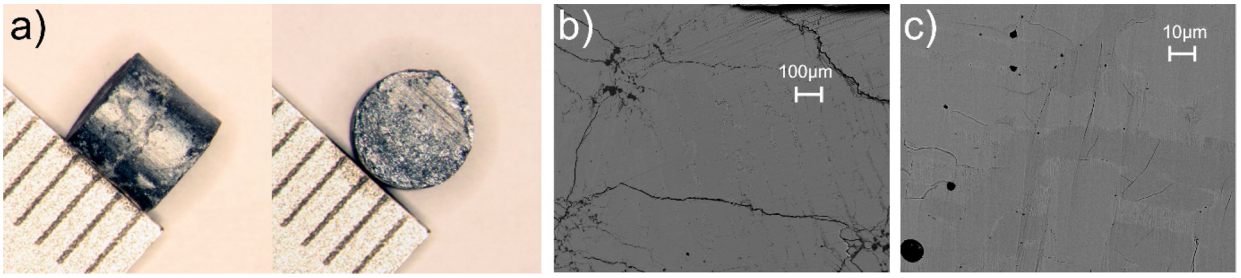

Figure 1. (a) Photograph of an as-synthesized cylindrical ZnAs specimen. SEM backscattered electron images of a cross-section polished surface at a magnification of ×100 (b) and of ×1000 (c). Black areas correspond to cracks and pores.

the PerkinElmer Instruments software, Pyris Software for Windows 3.51, and Pyris Thermal Analysis System Version 3.51.

Crystal Structure Characterization. A gray, dull, and irregularly shaped crystal (dimensions of 0.041 × 0.072 × 0.074 mm) was selected from a crushed part of a sample cylinder. Data were collected using a Bruker SMART-APEX diffractometer equipped with a D8 goniometer and an INCOATEC IμS Ag microsource (λ = 0.560 87 Å) employing Helios mirror optics. The crystal was measured at room temperature (300(2) K) and at 100(2) K with an Oxford cryostream cooling unit. The frames were integrated with the Bruker SAINT software package[20] using a narrow-frame algorithm. A numerical absorption correction was applied using SADABS.[21] Structure refinements were performed by using the JANA2006 package.[18] The assignment of Zn and As atoms having very similar X-ray scattering factors was based on the structure model of ZnSb. Table 1 lists a summary of the refinement results. Additional crystallographic information can be found in the Supporting Information.

Property Measurements. A bar-shaped specimen with approximate dimensions of 4 × 1 × 1 mm was cut from a cleaned and polished ZnAs cylinder (from the multianvil synthesis) using a wire saw. On this bar four gold-coated copper leads were connected via silver-filled epoxy (Epotek H31E) and silver paint in a four-probe setup. Seebeck coefficient, thermal conductivity, and electric resistivity were measured using the Thermal Transport Option (TTO) of the Physical Property Measurement System (PPMS) from Quantum Design. These measurements were done in vacuum (10^{-6} bar) in the temperature range of 2−400 K. Radiation heat loss was automatically corrected with the incorporated functions of the software for measurements using the TTO option. Heat capacity was measured between 300 and 2 K (50 points distributed logarithmically) using a quasi-adiabatic step heating technique as implemented in the PPMS. For heat capacity measurements a piece of a crushed cylinder (39.7 mg) was thermally connected to the platform of the sample-holder via a small amount of Apiezon-N grease (0.1 mg). The uncertainty for this measurement technique is estimated to be lower than 5%.

Spectroscopy Measurements. Optical diffuse reflectance measurements were performed with finely ground samples of ZnAs at room temperature. The spectrum was recorded in the region of 3200−10 500 cm^{-1} with a Bruker Equinox 55 FT-IR spectrometer equipped with a diffuse reflectance accessory (Harrick). Raman spectra of ZnAs and elemental As were measured using a Labram HR 800 spectrometer. The instrument is equipped with an 800 mm focal length spectrograph and an air-cooled (−70 °C), back-thinned CCD detector. Samples were excited using an air-cooled double frequency Nd:YAG laser (532 nm) and an input laser power of 5.6 mW (ZnAs) and 14 mW (As). Raman spectra were collected with an exposure time of 60 s, accumulation number of 10, and using an 1800 grooves/mm grating.

Computation. The phonon dispersion relations and thermodynamic functions of ZnAs were calculated via the Abinit program package[22−24] and employing the generalized gradient approximation (GGA) with the Perdew−Burke−Ernzerhof (PBE) parametrization.[25−27] GGA-PBE pseudopotentials were provided by the Abinit Web site. These pseudopotentials are norm-conserving and were generated using the fhi98PP package.[28] A 6 × 6 × 6 Monkhorst Pack[29] k-point grid was used for integration, and a 2 × 2 × 2 q-grid was used for calculations of the dynamical matrix elements. A planewave energy cutoff of 35 hartree (~950 eV) was employed. Prior to the phonon dispersion calculations ZnAs was structurally relaxed with respect to lattice parameters and atomic positions with forces converged to better than 1 × 10^{-3} eV/Å. From the phonon density of states (PDOS) it is possible to obtain the thermodynamic functions of a material.[30] Within the harmonic approximation the constant-volume specific heat C_V at temperature T is calculated as

$$C_v = 3nk_B \int_0^{\omega_L} \left(\frac{\hbar\omega}{2k_BT}\right)^2 \mathrm{csch}^2\left(\frac{\hbar\omega}{2k_BT}\right) g(\omega)\mathrm{d}\omega \quad (1)$$

where k_B is the Boltzmann constant, ω is the phonon frequency, ω_L is the highest frequency, n is the number of atoms in the unit cell, and $g(\omega)$ is the PDOS.

3. RESULTS AND DISCUSSION

Synthesis and Phase Relations. ZnAs was prepared from the elements by using high-pressure, high-temperature conditions. This is in accord with the finding of Clark and Range who employed a pressure of 4 GPa and a temperature of 1273 K in their synthesis.[9,10] However, when applying these conditions we obtained products containing substantial fractions of Zn_3As_2. The formation of Zn_3As_2 could be suppressed when applying higher pressures (around 6 GPa). We note that reactions were difficult to control and terminated frequently with blowouts when heating was performed at rates higher than 5 K/min and without intermediate holding steps.

Figure 1a shows a photograph of an as-obtained ZnAs specimen. The density was determined as 5.82 g/cm^3, which corresponds to 97.6% of the crystallographic density of ZnAs. SEM backscattered electron images of a polished surface are depicted in Figure 1b,c. These images reveal the presence of broad, micrometer-wide, cracks that extend 1 mm in length, as well as micrometer-sized pores. In addition, there is a large concentration of fine cracks (Figure 1c). Cylinder specimens obtained from high-pressure reactions could be easily crushed and disintegrated into a fine powder. EDX analysis of the area indicated in Figure 1c yielded 48.5 atom % Zn and 51.5 atom % As. This is in close agreement with the composition of the employed synthesis mixture, where a small excess of As was found to be advantageous for achieving products void of $ZnAs_2$ and Zn_3As_2. Figure 2 shows the PXRD pattern of this sample. The major impurity is As with about 2.5 wt %, which again reflects very well the starting composition. Binary oxides are barely detectable. However, it is possible that small amounts (<1 wt %) of other, not identifiable, impurities are present.

At ambient pressure ZnAs is metastable with respect to decomposition into Zn_3As_2 and $ZnAs_2$, which are the stable phases according to the Zn−As phase diagram.[2] Figure 3

dx.doi.org/10.1021/ic501308q | Inorg. Chem. 2014, 53, 8691−8699

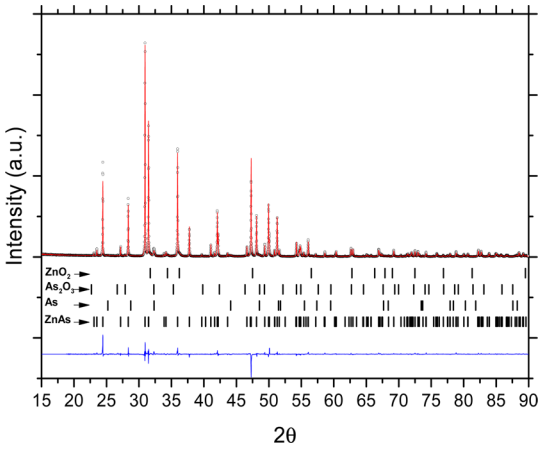

Figure 2. Rietveld fit to the PXRD pattern (Cu Kα_1) of as-synthesized ZnAs. Black circles and the red line represent measured and calculated diffraction patterns, respectively. The blue line corresponds to their difference. Refined wt % phase fractions: ZnAs−96.6(2), As−2.3(1), As_2O_3 − 0.3(1), ZnO − 0.7(1).

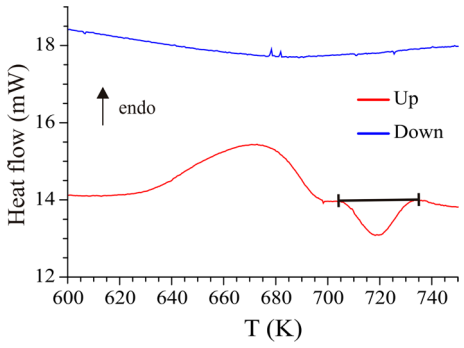

Figure 3. DSC heating (red line) and cooling trace (blue line) of ZnAs. The exothermic event corresponds to decomposition into $ZnAs_2$ and Zn_3As_2. The area of integration considered for enthalpy determination is indicated. The associated enthalpy is −3.6 J/g.

depicts DSC heating and cooling traces. Upon heating, a broad endothermic event occurs above 600 K, which is followed by a sharper exothermic one with an onset at 700 K and a maximum around 718 K. The latter event corresponds to decomposition of ZnAs with an enthalpy around −3.6 J/g. The PXRD pattern (see Supporting Information, Figure S1) of the decomposed sample after a DSC heating and cooling cycle fits approximately the expectation of an equimolar mixture; 4 ZnAs = $ZnAs_2$ + Zn_3As_2. The temperature of the exothermic decomposition depends on the heating rate or thermal history of the sample. Clark and Range reported a partial decomposition of ZnAs when performing annealing experiments for 17 h in a temperature range of 473−623 K, and complete decomposition occurred at higher temperatures.[9] The first thermal event in Figure 3 occurs reproducibly, but its origin is not clear. We attribute it to the presence of As in the sample, which segregates ("sweats") from the inside to the surface, and perhaps even oxidizes there. The sublimation temperature of As_2O_3 would fall in the temperature range of this event.

We conclude this section by recognizing that the synthesis of ZnAs by high-pressure conditions appears peculiar. At ambient pressure the molar volume of ZnAs exceeds the sum of atomic volumes of Zn and As (with respect to the elemental structures) by more than 6% (cf. Figure 4). Although this

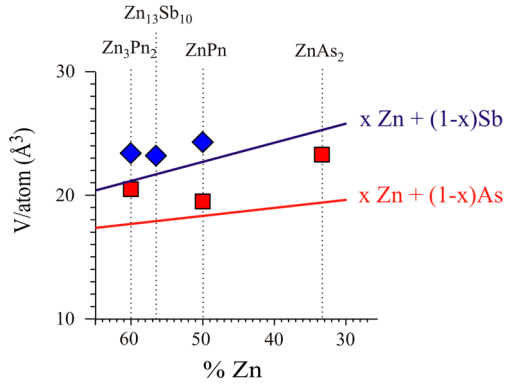

Figure 4. Molar volumes of zinc arsenide and antimonide phases (red and blue symbols, respectively) as compared to the weighted sum of atomic volumes with respect to the elemental structures (red and blue lines, respectively). Pn = As, Sb. $Zn_{13}Sb_{10}$ is the idealized crystallographic composition of Zn_4Sb_3.[3,16]

will be somewhat reduced at high pressures due to the rather high compressibility of As,[31] it can be safely stated that the pV term of the enthalpy is not favoring the formation of ZnAs from the elements. However, when instead referring to Zn_3As_2 and $ZnAs_2$—the thermodynamically stable compounds in the Zn−As system—a different result emerges. As shown in Figure 4 the molar volume of both stable compounds exceeds the sum of atomic volumes to an even larger extent than ZnAs. Consequently, the reaction Zn_3As_2 + $ZnAs_2$ = 4 ZnAs is actually accompanied by a volume reduction of almost 10% (172.4 Å^3 vs 156.2 Å^3). Therefore, it may be argued that ZnAs is obtained at high-pressure conditions because (i) compound/phase formation in the Zn−As system is generally strongly favored through the internal energy term of the enthalpy (e.g., we note that the melting point of Zn_3As_2 is considerably higher than that of Zn_3Sb_2, 1290 vs 840 K)[2] and (ii) compared to stable Zn_3As_2 and $ZnAs_2$ the molar volume of ZnAs shows a much smaller volume expansion with respect to the volumes of the elements (cf. Figure 4). It can be expected that ZnAs will decompose at pressures above 10 GPa. This is known for isostructural ZnSb, which undergoes pressure-induced decomposition into Zn and an alloy with an approximate composition of $Zn_{40}Sb_{60}$ at 7 GPa and room temperature.[32]

The phenomenon of volume increase upon compound formation is also observed for Zn−Sb phases, although less pronounced. It is in stark contrast to compound semiconductors exhibiting a larger degree of ionicity (e.g., Zintl phases), which typically show a pronounced volume decrease. The volume increase is in line with the covalent bonding scenario pursued earlier for ZnSb and ZnAs.[11] It is interesting to speculate whether Zn_4As_3, analogous to Zn_4Sb_3, can also be prepared at high pressures. Our synthesis efforts from the elements do not give any evidence. On the other hand Clark and Range reported the formation of a further quenchable Zn−As high-pressure phase when subjecting $ZnAs_2$ or mixtures of Zn_3As_2 and As to 4 GPa and 1473 K.[9,10] The composition and structure of this phase could not be characterized.

Crystal Structure Analysis. The previous structure determination of ZnAs was performed in 1976 and based on Guinier PXRD data.[10] In this work we succeeded to collect and refine high-resolution X-ray intensity data from a single crystal. Additionally Rietveld refinement of PXRD data was performed (for details see Supporting Information, Table S1). Tables 2

dx.doi.org/10.1021/ic501308q | Inorg. Chem. 2014, 53, 8691−8699

and 3 compare obtained structure parameters and interatomic distances, respectively.

Table 2. Lattice Parameters in Å, Unit Cell Volume in Å^3, Fractional Atomic Coordinates and Equivalent Atomic Displacement Parameters in Å^2 for ZnAs (space group *Pbca*) with Estimated Standard Deviations in Parentheses

parameter	SCXRD 100 K	SCXRD 300 K	Rietveld	ref 10
a	5.6607(3)	5.6731(1)	5.6768(2)	5.679(2)
b	7.2774(4)	7.2754(2)	7.2796 (2)	7.277(4)
c	7.5599(5)	7.5572(2)	7.5593(2)	7.559(4)
V	311.43(3)	311.92(1)	312.39(1)	312.4
x (Zn)	0.54016(3)	0.54145(3)	0.5409(7)	0.530
y (Zn)	0.61934(3)	0.62021(3)	0.6191(5)	0.614
z (Zn)	0.63509(2)	0.63546(3)	0.6360(5)	0.639
U_{iso}/U_{eq} (Zn)	0.00610(5)	0.01443(6)	0.036(2)	
x (As)	0.13827(3)	0.13820(3)	0.13096(6)	0.141
y (As)	0.07273(2)	0.07269(2)	0.0714(4)	0.076
z (As)	0.10086(2)	0.10084(2)	0.1007(4)	0.100
U_{iso}/U_{eq} (As)	0.00448(5)	0.00920(5)	0.027(1)	

Table 3. Selected Interatomic Distances in Å for ZnAs. Standard Deviations Are Given in Parentheses. Labeling of Zn−As Distances Refers to Figure 5c

atom pairs	SCXRD 100 K	SCXRD 300 K	Rietveld	ref 10
Zn−Zn	2.7195(3)	2.7336(3)	2.729(5)	2.70
Zn−As (c1)	2.4716(3)	2.4697(3)	2.489(5)	2.47
Zn−As (c2)	2.4994(3)	2.4985(3)	2.490(5)	2.49
Zn−As (r1)	2.5711(3)	2.5712(3)	2.571(5)	2.61
Zn−As (r2)	2.6826(3)	2.6966(3)	2.680(5)	2.62
As−As	2.4282(3)	2.4290(2)	2.431(5)	2.47

ZnAs crystallizes in an orthorhombic *Pbca* structure (CdSb type) which contains eight formula units in the unit cell. Both kinds of atoms are situated on Wyckoff sites 8c. The structure consists of edge-sharing $ZnAs_4$ tetrahedra that, in turn, are connected via common corners (Figure 5a,b). Each atom in the ZnAs structure attains a peculiar 5-fold coordination by one like and four unlike neighbors. At the same time each atom is also part of planar rhomboid rings Zn_2As_2. These rings contain a short Zn−Zn contact, which is a consequence of edge-sharing $ZnAs_4$ tetrahedra. A ring and its linkage to neighboring ones is shown in Figure 5c. This figure also compares the thermal ellipsoids at room temperature and 100 K. It is seen that the displacement parameters for Zn are larger and considerably more anisotropic than for As. This is especially the case at room temperature, whereas differences diminish at 100 K. When comparing further structure parameters at room temperature and 100 K one realizes only very small differences, which are virtually restricted to slight changes in the Zn positional parameters and the *a* lattice parameter. As a consequence the unit cell volume at 100 K is by only 0.2% smaller than at room temperature.

There are six distinct nearest-neighbor distances in the ZnAs structure, which are all captured within the rhomboid ring and its connectivity. According to Benson et al. the rhomboid ring represents a four-center, four-electron (4c4e) bonded entity that is connected via 2c2e bonds to neighboring rings.[11] This bonding model has also been applied to isostructural CdSb and ZnSb and provides an electron-precise situation for ZnAs based

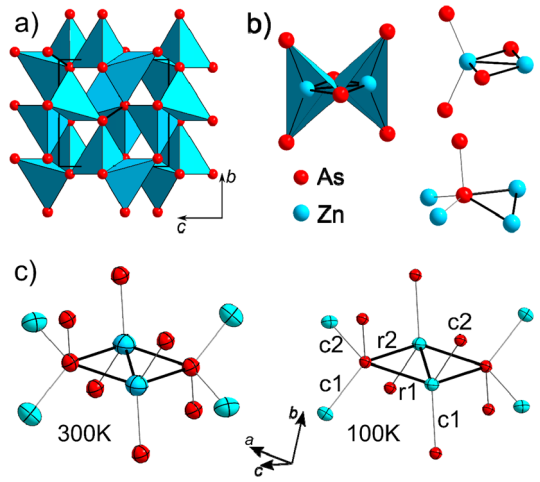

Figure 5. Crystal structure of ZnAs. (a) The quasi-tetrahedral coordination of Zn atoms by As is emphasized. (b) Edge-sharing arrangement of $ZnAs_4$ tetrahedra and five-coordination of Zn and As atoms. The rhomboid ring motif Zn_2As_2 is highlighted by bold bonds. (c) Rhomboid ring and its connectivity in the structure of ZnAs. The two different Zn−As distances within the ring (r1 and r2) and connecting rings (c1 and c2) are marked (cf. Table 3). The center of the ring corresponds to a center of inversion. Ellipsoids represent the experimentally determined thermal displacement parameters and are drawn at the 99.9% probability level (left for 300 K, right for 100 K). Zn atoms−cyan circles; As atoms−red circles.

on a covalent description. The different bonding motifs (rhomboid ring multicenter and connecting 2c2e) are well-reflected in the distribution of involved interatomic distances: Zn−As interatomic distances within a ring are about 0.1 Å larger than the ring connecting ones (cf. Table 3). The peculiarly short Zn−Zn distance (around 2.73 Å) is part of the multicenter bonding motif. The short As−As distance of around 2.43 Å corresponds to a ring-linking 2e2c bond. These nearest-neighbor distances associated with bonding interactions are well-separated from the next nearest ones, starting off above 3.5 Å.

We finally note that the results from the refinement of the single-crystal and PXRD room-temperature data are in close agreement. There is also a remarkable agreement between the previous refinement from Guinier powder data[10] and today's considerably more accurate ones. Significant deviations are only present for the Zn positional parameters.

Band Gap. Electronic band structure calculations predicted an indirect band gap with a size of 0.3 eV for ZnAs.[11] The measured diffuse reflectance *R* was transformed into the Kubelka−Munk remission function $F_{KM} = (1 - R^2)/2R$.[33] $F_{KM}(h\nu)$ for *R* of ZnAs is shown in Figure 6, together with $F_{KM}^{1/2}(h\nu)$, which is the transform characteristic for describing indirect allowed transitions along the absorption edge. Ideally F_{KM} is flat and has low values in the low-absorbance region at small photon energies.[34] This is not the case here, perhaps because of strong free carrier absorption or a high value of the refractory index. The band gap was estimated as the intersection of the straight-line extrapolations below and above the knee of the $F_{KM}^{1/2}$ curve.[34] The value is around 0.9 eV, which is substantially higher than the one obtained from first-principles calculations. It is also higher than the spectroscopically determined band gap for ZnSb (around 0.5 eV at room temperature).[35]

dx.doi.org/10.1021/ic501308q | Inorg. Chem. 2014, 53, 8691−8699

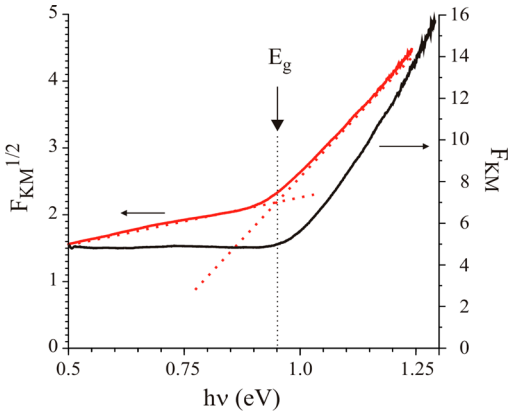

Figure 6. Spectral dependence of the Kubelka–Munk function (F_{KM}, black line) and the transform $F_{KM}^{1/2}$, red line). Straight broken lines fit the slopes of $F_{KM}^{1/2}$. The broken vertical line indicates the band gap at around 0.9 eV.

Transport Properties. The electrical resistivity of ZnAs decreases with increasing temperature as expected for a semiconductor (Figure 7a). However, instead of an exponential behavior, the decrease occurs rather linearly. Therefore, it was not possible to determine the band gap from resistivity data. In the region from 75 to 100 K an anomaly occurs, which is reproducibly observed upon temperature cycling and for other measured sample specimens. At room temperature the resistivity attains values around 1 Ω cm. Because of cracks present in the samples, resistivity values may not be correct on an absolute scale, and generally the results for the transport properties are to be regarded critically.

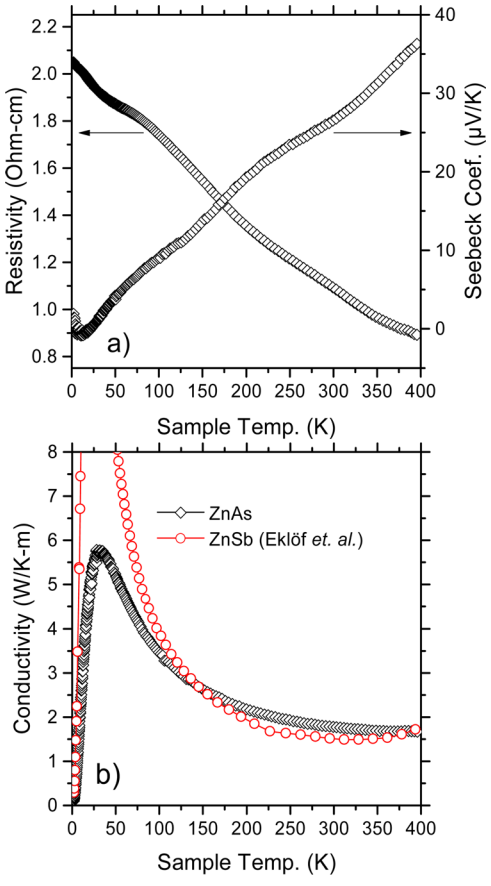

Figure 7. (a) Electrical resistivity, Seebeck coefficient, and (b) thermal conductivity of ZnAs. The thermal conductivity of ZnSb is shown for comparison (data from ref 37).

The Seebeck coefficient of ZnAs has a positive sign—implying holes as the major type of charge carriers—and exhibits an almost linear temperature dependence (also Figure 7a). This is similar to ZnSb; however, the value of +27 μV/K attained at room temperature is roughly an order of magnitude lower. The Goldsmid relation $E_g \approx 2eS_{max}T_{max}$,[36] which links the band gap and the Seebeck coefficient, holds roughly for ZnSb and would suggest a much higher Seebeck coefficient for ZnAs than the experimentally determined value. Again, sample imperfection (cracks, impurity phases) may lead to lower values than expected; however, the Seebeck coefficient may also be diminished by the presence of minority carriers from impurity bands. Figure 7b shows the thermal conductivity of ZnAs together with ZnSb (according to ref 37). In a highly crystalline semiconductor material the change between defect/boundary scattering and Umklapp scattering leads typically to a pronounced maximum upon heating.[38] Compared to ZnSb this maximum (seen at around 50 K for ZnAs) is not well-developed. This indicates that the ZnAs sample possesses highly fractured grains. Although absolute values are obscured by the presence of micrometer-sized cracks and impurities it appears that the thermal conductivity of ZnAs above 150 K (with values around 2 W/K·m) is very similar to ZnSb, which is composed of the heavier element Sb.[37]

Vibrational Properties. Figure 8a shows first-principles calculated phonon dispersion curves and the PDOS for ZnAs. The four modes at highest wavenumbers (at around 240 cm^{-1}) are only very weakly dispersed, which gives rise to a pronounced peak in the PDOS. These modes correspond to stretches within pairs of As atoms ("dumbbells"). There are four As_2 pairs in the unit cell. Modes that can be associated with inter-ring (c1 and c2) Zn–As atom pair stretches are distributed in the ranges from 200 to 230 cm^{-1} (8 modes) and from 170 to 200 cm^{-1} (8 modes). At lower wavenumbers inter-ring bends and vibrations within rhombohedral ring units mix. The PDOS shows that the contribution of As atoms to the displacements of modes with wavenumber below 170 cm^{-1} is significantly diminished. The phonon dispersion curves of ZnAs do not indicate peculiarities, like soft modes or a tendency to dynamical instability.

The Raman spectrum of ZnAs is shown in Figure 9 and is compared to elemental As. The complex ZnAs structure gives rise to 24 Raman active modes. Their analysis was attempted for CdSb,[39] but clear assignments proved difficult for other II–V compounds.[40] Seven bands can be discerned in our spectrum. The most intense one at 250 cm^{-1} is clearly attributed to the As–As stretches (calculated values are 240 cm^{-1} (B_{2g}), 239 cm^{-1} (B_{1g}), 237 cm^{-1} (A_g), 234 cm^{-1} (A_g)). The wavenumbers associated with these bands relate well to the A_g mode in elemental As. The rhombohedral structure of gray arsenic comprising puckered hexagon layers has two Raman active modes: the A_g mode where atoms displace along the C_3 axis, and the degenerate E_g mode where atoms displace perpendicular. Those are seen at 256 and 194 cm^{-1}, respectively. The bands observed at 72, 87, and 104 cm^{-1} for ZnAs (i.e., peaks 1–3 in Figure 9) can be associated with the weakly dispersed low-energy modes accumulating at the Γ point in the range of 70–100 cm^{-1} in Figure 8.

dx.doi.org/10.1021/ic501308q | Inorg. Chem. 2014, 53, 8691–8699

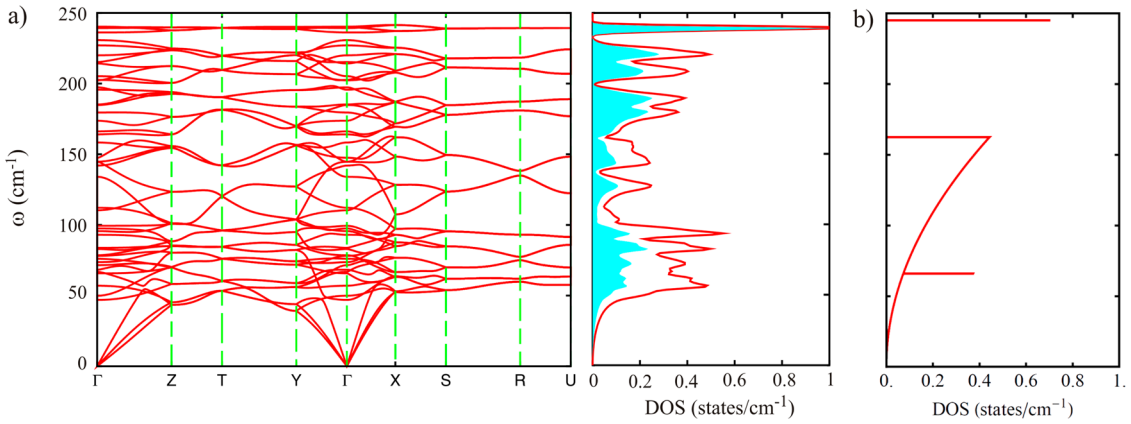

Figure 8. (a) Phonon dispersion (left) and phonon density of states (PDOS) of ZnAs (right). The As contribution to the PDOS is indicated by the cyan area. (b) PDOS model based on the Debye and Einstein temperatures as extracted from the measured heat capacity (cf. Figure 10). The height of the Einstein lines is arbitrary, but scaled to their respective contributions.

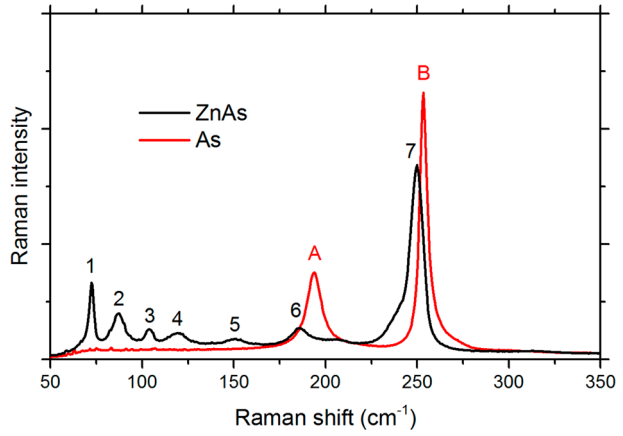

Figure 9. Raman spectrum of ZnAs and As recorded with an excitation wavelength of 532 nm. The values (in cm^{-1}) for the labeled bands 1−7 for ZnAs and A−B for As are as follows: 1:72, 2:87, 3:104, 4:120, 5:151, 6:186, 7:250, A:194 and B:256.

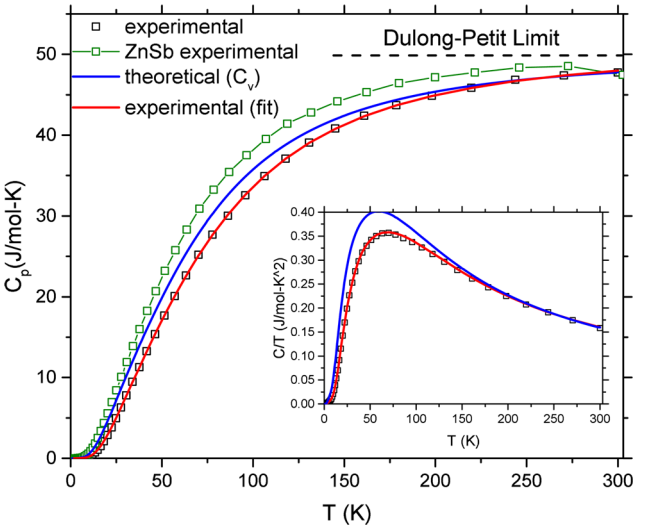

Figure 10. Specific heat C_p of ZnAs. Experimental data is shown as black squares, to which a Debye-Einstein fit was applied (red line, for details see text). Experimental data of ZnSb was added for comparison (connected green squares). The blue line is the computed constant volume specific heat C_v as obtained from the PDOS according to eq 1. (inset) C/T.

The heat capacity measurement, shown in Figure 10, does not indicate a phase transition at low temperatures for ZnAs. The room-temperature value of the specific heat, C_p, is about 48 J/mol·K and approaches the Dulong−Petit limit of 3R J/mol·atom·K (49.9 J/mol·K). The experimental data can be accurately modeled by a simple Debye−Einstein model, which assumes a Debye-type behavior for the three acoustic phonon branches and an Einstein (k-independent oscillator) behavior for the contributions from the optical branches.[41] Because of the presence of low-lying optical branches at least two different Einstein functions are necessary to model the phonon contributions to the specific heat. To be consistent with the lattice degrees of freedom the coefficient of the Debye contribution was kept at 3 R, while the coefficients of the Einstein functions were freely refined. The best fit was obtained with a Debye temperature Θ_D of 234 K, and the two Einstein temperatures Θ_{E1} = 95 K (66 cm^{-1}; 8.2 meV) and Θ_{E2} = 281 K (245 cm^{-1}; 30.4 meV) with coefficients 0.90 and 2.16 R, respectively. This fitted Debye temperature is lower than the one obtained in the low-temperature regime between 1.86 and 3.15 K, $\Theta_{D,LT}$ = 328 K. From this low-temperature region also a γ-value of 0.44 mJ/mol·K^2 could be estimated, which was kept constant during the fitting procedure. Both Einstein temperatures are well-reflected in the theoretical PDOS (cf. Figure 8a) by the presence of low-lying optical modes (Θ_{E1}) and the characteristic As−As stretches (Θ_{E2}). The model PDOS based on Θ_D, Θ_{E1}, and Θ_{E2} is shown as Figure 8b. The sum of the coefficients of the Debye and Einstein modes in our fitting model exceeds the ideal value of 6 R by 1%, which might be attributed to the presence of small As impurities, thermal lattice expansion, or experimental errors.

The specific heat capacity of ZnAs is also strikingly similar to isostructural ZnSb whose heat capacity is also shown in Figure 10. The heat capacity of ZnSb can be modeled in the same fashion with a related fitting model assuming a Debye temperature Θ_D of 188 K and the two Einstein temperatures Θ_{E1} = 72 K (50 cm^{-1}, 6.2 meV) and Θ_{E2} = 353 K (195 cm^{-1}, 25.4 meV) with coefficients of 0.96 and 2.10 R, respectively.

With knowledge of the PDOS the vibrational heat capacity at constant volume (C_v) can be calculated according to eq 1. The result is compared in Figure 10 with the measured heat capacity (C_p) of ZnAs. Above 150 K there is good agreement between experiment and theory. This phenomenon is due to the

dx.doi.org/10.1021/ic501308q | Inorg. Chem. 2014, 53, 8691−8699

underestimation of calculated wavenumbers, which is about 5% (cf. calculated As−As stretches at 240 cm^{-1} and corresponding Raman band at 250 cm^{-1}). At low temperatures underestimated phonon frequencies will lead to an overestimation of the heat capacity. At high temperatures, when the Dulong-Petit limit is approached, there must be agreement again, provided that contributions due to volume change and anharmonicity are small. The volume dependence of the heat capacity of ZnAs is considered negligible in the investigated temperature range because the crystallographic data suggest that thermal expansion is very small (cf. Table 2). The good agreement between calculated C_v and measured C_p above 150 K indicates further that the vibrational properties of ZnAs are essentially harmonic up to 300 K.

4. CONCLUSION

A reliable protocol for the synthesis of metastable ZnAs by multianvil high-pressure techniques at 6 GPa and 1273 K was established. ZnAs is isostructural to thermoelectric ZnSb, and both compounds are electron-poor II−V semiconductors featuring simultaneously multicenter and two-center bonding. The electrical transport properties of ZnAs are rather different from ZnSb, which can be mostly attributed to the larger band gap of ZnAs (0.9 eV vs 0.5 eV). The electrical resistivity of ZnAs shows a negative temperature dependence with values in the (Ω cm) range, whereas resistivity values of ZnSb are 2 orders of magnitude lower. Also the Seebeck coefficient of ZnAs is rather small compared to ZnSb (∼27 μV/K vs ∼300 μV/K at room temperature). Therefore, ZnAs cannot be considered a thermoelectric material. However, ZnAs exhibits a similarly low thermal conductivity as ZnSb although As is considerably lighter than Sb. Also the temperature dependence of the heat capacity of both compounds is very similar, which indicates very similar vibrational properties. These similarities probably originate in the common electron-poor bonding properties of both compounds. Multicenter bonded structural units (i.e., the rhomboid rings) give rise to a manifold of localized low-energy optical modes, and the interaction of those modes with the acoustic phonons can explain the low thermal conductivity of both materials.[6,42]

■ ASSOCIATED CONTENT

Supporting Information

Results of Rietveld analysis of ZnAs sample (Table S1), PXRD pattern of decomposed ZnAs (Figure S1), and crystallographic information in CIF files. This material is available free of charge via the Internet at http://pubs.acs.org. Additional crystallographic details can be obtained from the Fachinformationszentrum Karlsruhe, 76344 Eggenstein-Leopoldshafen, Germany, (fax: (49) 7247−808−666; e-mail: crysdata@fiz-karlsruhe.de) on quoting the depository numbers CSD-427612 (300 K) and CSD-427613 (100 K).

■ AUTHOR INFORMATION

Corresponding Author

*E-mail: Ulrich.Haussermann@mmk.su.se.

Present Address

[⊥]Department of Physics, Tsinghua University, Beijing, China, 100084

Notes

The authors declare no competing financial interest.

■ ACKNOWLEDGMENTS

This work was supported by the U.S. National Science Foundation (NSF-DMR-1007557), the Swedish Research Council (2010-4827 and 2013-4690), and the Deutsche Forschungsgemeinschaft (DFG, SCHE 478/12-1). We are grateful to Prof. U. Hålenius (Swedish Museum of Natural History, Stockholm) for assistance with the optical diffuse reflectance measurements.

■ REFERENCES

(1) Li, J.-B.; Record, M.-C.; Tedenac, J.-C. *J. Alloys Compd.* **2007**, *438*, 171−177.
(2) Massalski, T. B., Okamoto, H., ASM International. *Binary Alloy Phase Diagrams;* ASM International: Materials Park, OH, 1990.
(3) Snyder, G. J.; Christensen, M.; Nishibori, E.; Caillat, T.; Iversen, B. B. *Nat. Mater.* **2004**, *3*, 458−463.
(4) Toberer, E. S.; Rauwel, P.; Gariel, S.; Taftø, J.; Snyder, G. J. *J. Mater. Chem.* **2010**, *20*, 9877−9885.
(5) Iversen, B. B. *J. Mater. Chem.* **2010**, *20*, 10778−10787 and references therein.
(6) Jund, P.; Viennois, R.; Tao, X.; Niedziolka, K.; Tédenac, J.-C. *Phys. Rev. B* **2012**, *85*, 224105.
(7) Valset, K.; Böttger, P. H. M.; Taftø, J.; Finstad, T. G. *J. Appl. Phys.* **2012**, *111*, 023703.
(8) Xiong, D.-B.; Okamoto, N. L.; Inui, H. *Scr. Mater.* **2013**, *69*, 397−400.
(9) Clark, J. B.; Range, K.-J. *Z. Naturforsch., B* **1975**, *30*, 688−695.
(10) Clark, J. B.; Range, K.-J. *Z. Naturforsch., B* **1976**, *31*, 158−162.
(11) Benson, D.; Sankey, O. F.; Häussermann, U. *Phys. Rev. B* **2011**, *84*, 125211.
(12) Turner, W. J.; Fischler, A. S.; Reese, W. E. *Phys. Rev.* **1961**, *121*, 759−767.
(13) Turner, W. J.; Fischler, A. S.; Reese, W. E. *J. Appl. Phys.* **1961**, *32*, 2241−2245.
(14) Nasledov, D. N.; Shevchenko, V. Y. *Phys. Status Solidi A* **1973**, *15*, 9−38.
(15) Arushanov, E. K. *Prog. Cryst. Growth Charact.* **1986**, *13*, 1−38.
(16) Mikhaylushkin, A. S.; Nylen, J.; Häussermann, U. *Chem.—Eur. J.* **2006**, *37*, 4912−4920.
(17) Stoyanov, E.; Häussermann, U.; Leinenweber, K. *High Pressure Res.* **2010**, *30*, 175−189.
(18) Petricek, V.; Dusek, M.; Palatinus, L. *Jana2006, The Crystallographic Computing System;* Academy of Sciences: Praha, Czech Republic, 2006.
(19) *CASINO v2.48, Monte Carlo Simulation of Electron Trajectory in Solids;* Université de Sherbrooke: Québec, Canada, 2011.
(20) *SAINT v7.68A;* Bruker AXS Inc.: Madison, WI, USA, 2008.
(21) Sheldrick, G. M. *SADABS v2008/2;* University of Göttingen: Göttingen, Germany, 2008.
(22) Gonze, X. *Z. Kristallogr.* **2005**, *220*, 558−562.
(23) Gonze, X.; Amadon, B.; Anglade, P.-M.; Beuken, J.-M.; Bottin, F.; Boulanger, P.; Bruneval, F.; Caliste, D.; Caracas, R.; Côté, M.; Deutsch, T.; Genovese, L.; Ghosez, P.; Giantomassi, M.; Goedecker, S.; Hamann, D. R.; Hermet, P.; Jollet, F.; Jomard, G.; Leroux, S.; Mancini, M.; Mazevet, S.; Oliveira, M. J. T.; Onida, G.; Pouillon, Y.; Rangel, T.; Rignanese, G.-M.; Sangalli, D.; Shaltaf, R.; Torrent, M.; Verstraete, M. J.; Zerah, G.; Zwanziger, J. W. *Comput. Phys. Commun.* **2009**, *180*, 2582−2615.
(24) Gonze, X.; Beuken, J.-M.; Caracas, R.; Detraux, F.; Fuchs, M.; Rignanese, G.-M.; Sindic, L.; Verstraete, M.; Zerah, G.; Jollet, F.; Torrent, M.; Roy, A.; Mikami, M.; Ghosez, P.; Raty, J.-Y.; Allan, D. C. *Comput. Mater. Sci.* **2002**, *25*, 478−492.
(25) Wang, Y.; Perdew, J. P. *Phys. Rev. B* **1991**, *44*, 13298−13307.
(26) Perdew, J. P.; Chevary, J. A.; Vosko, S. H.; Jackson, K. A.; Pederson, M. R.; Singh, D. J.; Fiolhais, C. *Phys. Rev. B* **1992**, *46*, 6671−6687.
(27) Perdew, J. P.; Burke, K.; Ernzerhof, M. *Phys. Rev. Lett.* **1996**, *77*, 3865−3868.

(28) Fuchs, M.; Scheffler, M. *Comput. Phys. Commun.* **1999**, *119*, 67−98.
(29) Monkhorst, H. J.; Pack, J. D. *Phys. Rev. B* **1976**, *13*, 5188−5192.
(30) (a) Ke, X.; Tanaka, I. *Phys. Rev. B* **2005**, *71*, 024117. (b) Stoffel, R. P.; Wessel, C.; Lumey, M.-W.; Dronskowski, R. *Angew. Chem., Int. Ed.* **2010**, *49*, 5242−5266.
(31) Morosin, B.; Schirber, J. E. *Solid State Commun.* **1972**, *10*, 249−251.
(32) (a) Degtyareva, V. F.; Bdikin, I. K.; Khasanov, S. S. *Phys. Solid State* **1997**, *39*, 1341−1344. (b) Degtyareva, V. F.; Degtyareva, O.; Mao, H.; Hemley, R. J. *Phys. Rev. B* **2006**, 214108.
(33) (a) Kubelka, P.; Munk, F. *Z. Technol. Phys.* **1931**, *12*, 593−599. (b) Kubelka, P. *J. Opt. Soc. Am.* **1948**, *38*, 448−457. (c) Philips-Invernizzi, B.; Cazé, C.; Dupont, D. *Opt. Eng.* **2001**, *40*, 1082−1092.
(34) Nowak, M.; Kauch, B.; Szperlich, P. *Rev. Sci. Instrum.* **2009**, *80*, 046107.
(35) (a) Závêtová, M. *Phys. Status Solidi B* **1964**, *5*, K19−K21. (b) Komiya, H.; Masumoto, K.; Fan, H. Y. *Phys. Rev.* **1964**, *133*, A1679−A1684.
(36) Goldsmid, H. J.; Sharp, J. W. *J. Electron. Mater.* **1999**, *28*, 869−872.
(37) Eklöf, D.; Fischer, A.; Wu, Y.; Scheidt, E.-W.; Scherer, W.; Häussermann, U. *J. Mater. Chem. A* **2012**, *1*, 1407−1414.
(38) (a) Slack, G. A. In *Solid State Physics;* Ehrenreich, H., Seitz, F., Turnbull, D., Eds.; Academic Press: Waltham, MA, 1979; Vol. *34*, pp 1−71. (b) *Thermal Conductivity: Theory, Properties, and Applications (Physics of Solids and Liquids);* Tritt, T. M., Ed.; Springer: New York, NY, 2004.
(39) (a) Smirnov, D. V.; Mashovets, D. V.; Pasquier, S.; Leotin, J.; Puech, P.; Landa, G.; Roznovan, Y. V. *Semicond. Sci. Technol.* **1994**, *9*, 333−337. (b) Houde, D.; Lefaivre, J.; Jandl, S.; Arushanov, E. *Solid State Commun.* **1982**, *41*, 325−327.
(40) Trichês, D. M.; Souza, S. M.; de Lima, J. C.; Grandi, T. A.; Campos, C. E. M.; Polian, A.; Itié, J. P.; Baudelet, F.; Chervin, J. C. *J. Appl. Phys.* **2009**, *106*, 013509.
(41) Kelley, K. K.; King, E. G. *Contributions to the Data on Theoretical Metallurgy: Part 14. Entropies of the Elements and Inorganic Compounds;* Technical Report Bulletin 592 (U.S. Bureau of Mines) for the U.S. Government Printing Office:Washington, DC, 1961.
(42) Bjerg, L.; Iversen, B. B.; Madsen, G. K. H. *Phys. Rev. B* **2014**, *89*, 024304.

dx.doi.org/10.1021/ic501308q | *Inorg. Chem.* 2014, 53, 8691−8699